INSTITUTE OF PHYSICS PUBLISHING JOURNAL OF OPTICS B: QUANTUM AND SEMICLASSICAL OPTICS
J. Opt. B: Quantum Semiclass. Opt. **7** (2005) 235–239 doi:10.1088/1464-4266/7/9/001

The spatial shape of entangled photon states generated in non-collinear, walking parametric downconversion

Juan P Torres[1,2], **Gabriel Molina-Terriza**[1] **and Lluis Torner**[1,2]

[1] ICFO-Institut de Ciencies Fotoniques, Barcelona 08034, Spain
[2] Department of Signal Theory and Communications, Universitat Politecnica de Catalunya, Barcelona 08034, Spain

Received 17 March 2005, accepted for publication 27 April 2005
Published 2 August 2005
Online at stacks.iop.org/JOptB/7/235

Abstract
We address the spatial shape of entangled photon states generated in spontaneous parametric downconversion in non-collinear geometries, when the interacting waves exhibit Poynting vector walk-off. We discuss how such shape depends on the interplay between the state ellipticity caused by the non-collinear geometry, and the Poynting vector walk-off. In particular, we study the impact of the new features exhibited by walking entangled photons on the implementation of quantum protocols based on the *spiral spectra* of the entangled photons.

Keywords: parametric downconversion, orbital angular momentum of light

Spontaneous parametric downconversion (SPDC) is a reliable source of entangled photons. The generated two-photon states exhibit, in particular, spatial entanglement embedded in the corresponding mode function. The spatial structure of the two-photon state provides a new resource to explore quantum physics beyond the two-dimensional Hilbert space generated by the polarization state of the photons. The corresponding multidimensional entangled states, or qudits, can be encoded in orbital angular momentum (OAM) [1], thus providing infinite-dimensional alphabets [2], which can be used to conduct proof-of-principle demonstrations of quantum protocols whose implementation requires higher-dimensional Hilbert spaces. Illustrative examples include the violation of Bell inequalities with qutrits [3], and the implementation of a quantum coin tossing protocol [4].

Two-photon entangled states with well defined spatial properties, e.g., qutrits encoded in a well defined value of OAM [5, 6], are not harvested directly at the output of the downconverting crystal, thus elucidation of techniques to generate the appropriate states are required. In general, the implementation of a d-dimensional quantum channel requires the generation of arbitrary engineered entangled states, thus controlling such structures is of paramount importance for many applications, including, e.g., those addressed to multidimensional quantum imaging [7]. An appropriate tailoring of the mode function of the two-photon state requires the consideration of all parameters that effectively determine its spatial shape. Importantly, in certain regions of the parameter space that define the SPDC process, some of these parameters might be neglected, or alternatively have their importance enhanced.

In a typical SPDC configuration, a strong pump interacts with a nonlinear $\chi^{(2)}$ crystal, generating a pair of photons that propagate at a certain angle. Most previous investigations of entangled photons addressed nearly collinear phase-matching geometries in which pump, signal and idler photons propagate almost along the same direction. Actually, in genuine non-collinear geometries both the spin angular momentum [8], and the orbital angular momentum of the entangled photons depend strongly on the propagation direction of the photons. The impact of such effects on the OAM can be made important even when only purely geometrical features are considered [9], and can become dominant in the case of highly non-collinear settings such as transverse-emitting configurations [10], or for highly focused pump beams [11]. The presence of Poynting vector walk-off due to crystal birefringence is also expected to greatly impact the spatial structure of the entangled quantum state, as we confirm here.

Here we show that the spatial shape of the two-photon state results from the interplay between the effects on the spatial shape due to the non-collinear geometry and due to the Poynting vector walk-off. The importance of both effects

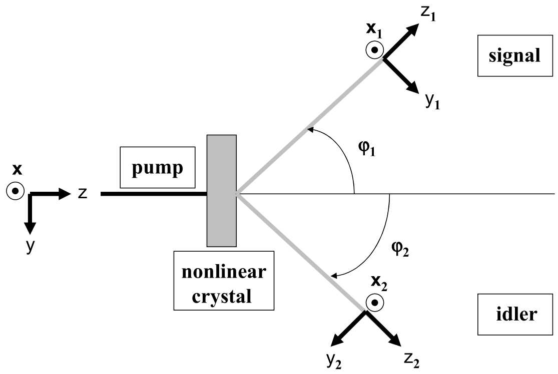

Figure 1. Schematic diagram of a non-collinear spontaneous parametric downconversion process in a nonlinear crystal.

mainly depends on the angle of emission of the photons, and on the value of the Poynting vector walk-off which is dictated by the beam width of the pump beam and the length of the nonlinear crystal. Our results are consistent with the observations reported to date (see, in particular [1, 12]), where a large enough pump beam width renders non-collinear and Poynting vector walk-off effects small, and with the recent observations reported by Altman and co-workers [11], and predict several additional new features.

We consider a nonlinear uniaxial crystal, such as BBO or $LiNbO_3$, in a type I (*ooe*) SPDC configuration, commonly used for the generation of spatially entangled two-photon states. The crystal is illuminated by a quasimonochromatic laser pump beam propagating in the z direction (figure 1). The downconverted photons propagate in the yz plane, and show no Poynting vector walk-off, while the pump beam does. The optics axis of the nonlinear crystal and the z axis are contained in a plane that forms an angle α with the yz plane. The optics axis forms an angle ν_0 with the propagation direction of the pump beam, z. The angle ν_0 determines the angle of the cone where the downconverted photons are emitted, and the angle α determines the azimuthal position inside the cone where the photons will be detected. The two-photon quantum state $|\Psi\rangle$ at the output of the nonlinear crystal, within the first order perturbation theory, is given by $|\Psi\rangle = |0,0\rangle - \mathrm{i}/\hbar \int_0^\tau \mathrm{d}t\, H_\mathrm{I}(t)|0,0\rangle$, where $|0,0\rangle$ is the vacuum state, τ is the interaction time, and $H_\mathrm{I}(t)$ is the effective Hamiltonian in the interaction picture, given by $H_\mathrm{I} = \epsilon_0 \int_V \mathrm{d}^3V\, \chi^{(2)} E_\mathrm{p}^+ E_\mathrm{s}^- E_\mathrm{i}^- + \text{c.c}$, where E_p^+ refers to the positive-frequency part of the pump electric field operator and $E_\mathrm{s,i}^-$ refers to the negative-frequency part of the signal and idler electric field operators.

The amplitude field profile of the paraxial pump beam, which is treated classically, is written $E_\mathrm{p}^+(\mathbf{x}, z, t) = \int \mathrm{d}\mathbf{q}_\mathrm{p}\, E_0(\mathbf{q}_\mathrm{p}) \exp[\mathrm{i}k_\mathrm{p}z + \mathrm{i}(\mathbf{x}+z\boldsymbol{\rho}_0)\cdot\mathbf{q}_\mathrm{p} - \mathrm{i}\omega_\mathrm{p}t]$, where $\mathbf{x} = (x, y)$ is the position in the transverse plane, $\mathbf{q}_\mathrm{p}$ is the transverse wavevector, ω_p is the angular frequency of the pump beam, $\boldsymbol{\rho}_0 = (\tan\rho_0\cos\alpha, \tan\rho_0\sin\alpha)$ is the value of the spatial walk-off, $E_0(\mathbf{q}_\mathrm{p})$ is the field profile of the pump beam in momentum space, and $k_\mathrm{p} = \sqrt{(k_\mathrm{p}^0)^2 - |\mathbf{q}_\mathrm{p}|^2}$ is the longitudinal wavenumber inside the crystal. In an uniaxial crystal, the refractive index of an extraordinary plane wave is known to depend on the angle formed by the direction of propagation of the wave and the optic axis of the crystal $(\nu_0 + \Delta\nu)$, thus $|\mathbf{k}_\mathrm{p}| = \omega_\mathrm{p} n_\mathrm{p}(\nu_0 + \Delta\nu)/c$. In currently used nonlinear crystals [14], the change of refractive index for small angle deviations from the central wavevector fulfils $(1/n_\mathrm{p}(\nu_0))(\partial n_\mathrm{p}/\partial\nu)_{\nu_0}\Delta\nu \ll 1$, so that we can write $|\mathbf{k}_\mathrm{p}| = k_\mathrm{p}^0$, where $k_\mathrm{p}^0 = \omega_\mathrm{p} n_\mathrm{p}(\nu_0)/c$.

In order to devise the spatial structure of the generated two-photon state, we define $\mathbf{x}_{1,2} = \mathbf{x}$, $\mathbf{y}_{1,2} = \mathbf{y}\cos\varphi_{1,2} + \mathbf{z}\sin\varphi_{1,2}$ and $\mathbf{z}_{1,2} = \mathbf{z}\cos\varphi_{1,2} - \mathbf{y}\sin\varphi_{1,2}$, where $\varphi_{1,2}$ are the angles formed by the direction of propagation of the pump beam (z) and the direction of propagation of the signal (z_1) and idler photons (z_2), respectively. Because of the phase matching conditions imposed by the nonlinear crystal, the central wavevectors of the downconverted photons can be written as $\mathbf{k}_\mathrm{s}^0 = (\omega_\mathrm{s} n_\mathrm{s}/c)[\cos\varphi_1\mathbf{z} - \sin\varphi_1\mathbf{y}]$, and $\mathbf{k}_\mathrm{i}^0 = (\omega_\mathrm{i} n_\mathrm{i}/c)[\cos\varphi_2\mathbf{z} - \sin\varphi_2\mathbf{y}]$, with c being the velocity of light in vacuum, $\omega_\mathrm{s,i}$ the angular frequency of the signal (idler) photon, and $n_\mathrm{s,i}$ the refractive index inside the nonlinear crystal at the signal (idler) wavelength. Since we are interested in the spatial structure of the downconverted photons, we consider that the wavevectors of the signal and idler photons belong to a narrow bundle around the corresponding central wavevectors [13], i.e., $\mathbf{k}_\mathrm{s} = \mathbf{k}_\mathrm{s}^0 + \Delta\mathbf{k}_\mathrm{s}$ and $\mathbf{k}_\mathrm{i} = \mathbf{k}_\mathrm{i}^0 + \Delta\mathbf{k}_\mathrm{i}$, with $|\Delta\mathbf{k}_\mathrm{s}| \ll |\mathbf{k}_\mathrm{s}^0|$ and $|\Delta\mathbf{k}_\mathrm{i}| \ll |\mathbf{k}_\mathrm{i}^0|$. Therefore, in the $(\mathbf{x}_1, \mathbf{y}_1, \mathbf{z}_1)$ system, we can write $\mathbf{k}_\mathrm{s} = p_x\mathbf{x}_1 + p_y\mathbf{y}_1 + k_\mathrm{s}\mathbf{z}_1$. We have defined the transverse momentum for the signal photon as $\mathbf{p} = (p_x, p_y)$, and $k_\mathrm{s} = \sqrt{(k_\mathrm{s}^0)^2 - |\mathbf{p}|^2}$, with $k_\mathrm{s}^0 = \omega_\mathrm{s} n_\mathrm{s}/c$. A similar expression can be written for the idler photon.

The electric field amplitude operator corresponding to the signal photon E_s^- can be written as $E_\mathrm{s}^-(\mathbf{x}, z, t) \propto \int \mathrm{d}\mathbf{p} \exp\{-\mathrm{i}k_\mathrm{s}z_1 - \mathrm{i}\mathbf{p}\cdot\mathbf{x}_1 + \mathrm{i}\omega_\mathrm{s}t\} a_\mathrm{s}^+(\mathbf{p})$, where $\mathbf{x}_1 = (x_1, y_1)$ is the position in the transverse plane of the signal photon, and a_s^+ is the creation operator of a signal photon with transverse wavevector $\mathbf{p}$. For the idler photon, we can write a similar expression, with $\mathbf{x}_2 = (x_2, y_2)$ being the transverse coordinates, $\mathbf{q} = (q_x, q_y)$ the transverse wavevector, $k_\mathrm{i} = \sqrt{(k_\mathrm{i}^0)^2 - |\mathbf{q}|^2}$ the longitudinal wavenumber, and $k_\mathrm{i}^0 = \omega_\mathrm{i} n_\mathrm{i}(\nu_0)/c$.

The quantum state of the two-photon state (excluding vacuum) is written [10, 13]

$$|\Psi\rangle = \int \mathrm{d}\mathbf{p}\,\mathrm{d}\mathbf{q}\, \Phi(\mathbf{p}, \mathbf{q}) a_\mathrm{s}^\dagger(\mathbf{p}) a_\mathrm{i}^\dagger(\mathbf{q})|0,0\rangle, \tag{1}$$

with

$$\Phi(\mathbf{p}, \mathbf{q}) = E_0(p_x + q_x, \Delta_0)\,\mathrm{sinc}(\Delta_k L/2)\exp(\mathrm{i}\Delta_k L/2), \tag{2}$$

where L is the crystal length,

$$\begin{aligned}\Delta_k &= k_\mathrm{p} - k_\mathrm{s}\cos\varphi_1 - k_\mathrm{i}\cos\varphi_2 + (p_x + q_x)\tan\rho_0\cos\alpha \\ &\quad + \Delta_0\tan\rho_0\sin\alpha - p_y\sin\varphi_1 - q_y\sin\varphi_2,\end{aligned} \tag{3}$$

comes from the phase matching condition in the z direction, and

$$\Delta_0 = p_y\cos\varphi_1 + q_y\cos\varphi_2 - k_\mathrm{s}\sin\varphi_1 - k_\mathrm{i}\sin\varphi_2. \tag{4}$$

The wavenumber of the pump beam is written $k_\mathrm{p} = \sqrt{(k_\mathrm{p}^0)^2 - (p_x + q_x)^2 - \Delta_0^2}$. The signal and idler photons are assumed to be monochromatic, with $\omega_\mathrm{p} = \omega_\mathrm{s} + \omega_\mathrm{i}$. This assumption is justified by the use of narrowband interference filters in front of the detectors.

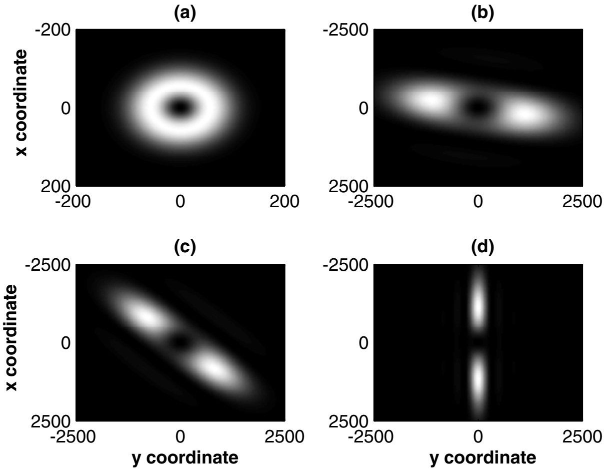

Figure 2. Spatial shape (coincidence rate) of the mode function of the signal photon for $\alpha = 0°$. (a) $w_0 = 800\ \mu$m and $\varphi_1 = 1°$, (b) $w_0 = 40\ \mu$m and $\varphi_1 = 1°$, (c) $w_0 = 40\ \mu$m and $\varphi_1 = 5°$, and (d) $w_0 = 40\ \mu$m and $\varphi_1 = 17.1°$. Length of the crystal: $L = 2$ mm. In all cases $\varphi_1 = -\varphi_2$. Focal length of the 2-f system: $f = 25$ cm. Units are in μm.

For a collinear configuration ($\varphi_1 = \varphi_2 = 0$), and neglecting the Poynting vector walk-off of all interacting beams, the mode function given in equation (2) is written [15, 16] $\Phi(\mathbf{p}, \mathbf{q}) \propto E_0(\mathbf{p} + \mathbf{q})\,\mathrm{sinc}[|\mathbf{p} - \mathbf{q}|^2 L/(4k_p^0)]\exp[\mathrm{i}|\mathbf{p} - \mathbf{q}|^2 L/(4k_p^0)]$, where one should make use of the paraxial approximation $k_p \sim k_p^0 - |\mathbf{p}|^2/(2k_p^0)$, and correspondingly for the signal and idler wavevectors. For this case, it has been shown [16] that if the spatial shape of the pump beam corresponds to a vortex beam with winding number l_0, and we project the idler photon into a mode with winding number l_2, the OAM content of the signal photon present a single peak at l_1, so that it fulfils the selection rule

$$l_0 = l_1 + l_2. \tag{5}$$

A similar result has been obtained under the thin crystal approximation [17], where the mode function is now written as $\Phi(\mathbf{p}, \mathbf{q}) \propto E_0(\mathbf{p} + \mathbf{q})$.

The signal and idler photons traverse two identical 2-f systems, with focal length $f_s = f_i = f$. The observation planes are assumed to be located at the focal length of the lens, $z_1 = z_2 = f$. The 2-f system provides a spatial image of the two-photon state $\Phi(\mathbf{p}, \mathbf{q})$, so that by measuring coincidence rates at different positions in the transverse plane one obtains information about the spatial shape of the mode function [18]. The probability to detect an idler photon at position $\mathbf{x}_2$ in coincidence with a signal photon at position $\mathbf{x}_1$ is given by $R_c(\mathbf{x}_1, \mathbf{x}_2) = |\Phi[2\pi\mathbf{x}_1/(\lambda f), 2\pi\mathbf{x}_2/(\lambda_i f)]|^2$. If the idler photon is projected into a plane-wave mode with $\mathbf{q} = 0$, which is experimentally realized by locating a small pinhole at $\mathbf{x}_2 = 0$ in the focal plane, the mode function $\Phi_s(\mathbf{p})$ of the signal photon turns out to be $\Phi_s(\mathbf{p}) = \Phi(\mathbf{p}, \mathbf{q} = 0)$. Projection into the mode $\mathbf{q} = 0$ is equivalent to projection of the idler photon into a Gaussian mode with a very large beam width, i.e., $\Phi_s(\mathbf{p}) \propto \int \mathrm{d}\mathbf{q}\,\Phi(\mathbf{p}, \mathbf{q})\exp(-|\mathbf{q}|^2 w_1^2/4)$, where $w_1 \to \infty$ is the width of the Gaussian mode. Thus the configuration described here performs a projection of the idler photon onto a mode with $l_2 = 0$.

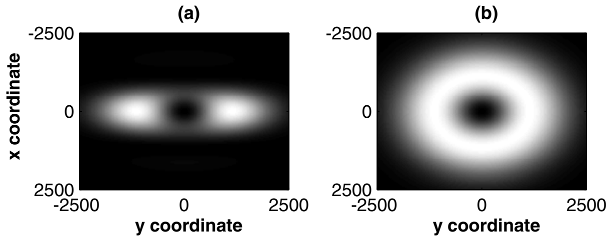

Figure 3. Spatial shape (coincidence rate) of the mode function of the signal photon. (a) $\alpha = 11.75°$ and $\varphi_1 = 1°$, (b) $\alpha = 90°$ and $\varphi_1 = 5°$. Length of the crystal: $L = 2$ mm and $w_0 = 40\ \mu$m. In all cases $\varphi_1 = -\varphi_2$. Focal length of the 2-f system: $f = 25$ cm. Units are in μm.

In figures 2 and 3 we plot the spatial shape of the signal photon. More specifically, we plot the coincidence rate $R_c(\mathbf{x}_1, \mathbf{x}_2 = 0)$, which gives us the intensity of the mode function. As an illustrative example, we consider a $LiIO_3$ crystal with length $L = 2$ mm. The pump beam is written $E_0(\mathbf{p}) \propto (p_x + \mathrm{i}p_y)\exp(-|\mathbf{p}|^2 w_0^2/4)$, which corresponds to a vortex beam with winding number $l_0 = 1$ and pump beam width w_0. In all cases considered, the diffraction length of the pump beam, $L_d = k_p^0 w_0^2/2$, is assumed to be much larger than the crystal length ($L_d \gg L$). Under this condition, if we make use of the paraxial approximation in equations (3) and (4),the mode function of the signal photon can be written as

$$\begin{aligned}\Phi_s(\mathbf{p}) \propto E_0(p_x, p_y\cos\varphi_1)\,\mathrm{sinc}&\left\{[p_x \tan\rho_0\cos\alpha\right.\\ &\left.+\, p_y\,(\tan\rho_0\cos\varphi_1\sin\alpha - \sin\varphi_1)]\,\frac{L}{2}\right\}\\ \times\ \exp&\left\{\mathrm{i}\,[p_x\tan\rho_0\cos\alpha\right.\\ &\left.+\, p_y\,(\tan\rho_0\cos\varphi_1\sin\alpha - \sin\varphi_1)]\,\frac{L}{2}\right\}.\end{aligned} \tag{6}$$

Therefore, the intensity of the mode function of the signal photon, $|\Phi_s(\mathbf{p})|^2$, is strongly affected by the slope in the (p_x, p_y) plane of the loci of perfect phase matching transverse momentum, which is written

$$\frac{p_x}{p_y} = \frac{\sin\varphi_1 - \tan\rho_0\cos\varphi_1\sin\alpha}{\tan\rho_0\cos\alpha}. \tag{7}$$

As is readily apparent, this expression turns out to be determined by the relationship between three angles: the angles that determine the direction of emission of the downconverted photons, φ_1 and α, and the walk-off angle of the pump beam, ρ_0.

In figure 2, we plot the spatial shape of the signal photon for some representative cases corresponding to $\alpha = 0°$. In this case, the downconverted photons propagate in a plane perpendicular to the plane formed by the optics axis and the direction of propagation of the pump beam. Perfect phase matching is achieved for values of the transverse momentum so that $p_x/p_y = L_w/L_{nc}$, where $L_{nc} = w_0/\sin\varphi_1$ is the non-collinear length and $L_w = w_0/\tan\rho_0$ is the walk-off length of the pump beam. In figure 2(a), the width of the pump beam is very large ($w_0 = 800\ \mu$m), so that both the non-collinear length and the walk-off length are much larger than the crystal length ($L \ll L_{nc}, L_w$). The coincidence rate

$R_c(\mathbf{x_1}, \mathbf{x_2} = 0)$, which is cylindrically symmetric, mirrors the shape of the intensity of the pump beam. In this case, the effects of the spatial walk-off of the pump beam and the non-collinear geometry are negligible.

In contrast, when the width of the pump beam decreases so that L_{nc} and L_w become comparable to or smaller than the crystal length, the coincidence rate no longer mimics the spatial shape of the pump beam, so as to show a break-up of the cylindrical symmetry. This ellipticity can be observed in figures 2(b) and (c), where the pump beam width is $w_0 = 40\ \mu$m. In figures 2(a) and (b) the angle of emission of the signal photon is $\varphi_1 = 1°$, while in figure 2(c) it is $\varphi_1 = 5°$. If $L_w \to \infty$, which corresponds to a configuration where the Poynting vector walk-off is negligible, the loci of perfect phase matching is the direction $p_y = 0$, as it is shown in figure 2(d). This is the case when the direction of propagation of the pump beam ($\mathbf{z}$) forms an angle $\nu_0 = 90°$ with the optic axis of the crystal. It is also the case for most QPM configurations used for SPDC [19, 20].

In figure 3(a) we plot a case where the locus of perfect phase matching corresponds to $p_x = 0$. From equation (7), we see that this turns out to be the case when $\sin\alpha = \tan\varphi_1/\tan\rho_0$. The effects on the spatial shape of the signal photon due to the non-collinear emission in SPDC and to the presence of Poynting vector walk-off can compensate each other, as shown in figure 3(b), where the cylindrical symmetry is restored, even when the non-collinear and walk-off lengths are smaller than the crystal length. For $\alpha = 90°$, the optics axis of the nonlinear crystal is contained in the plane yz, where the downconverted photons propagate. Therefore, for $\sin\varphi_1 \sim \tan\rho_0$, both effects cancel each other.

Most implementations of quantum protocols based on spatial entanglement put forward to date make use of the OAM to encode quantum information [3, 4]. To represent spatial entanglement in terms of OAM one employs spatial modes with an azimuthal phase dependence of the form $\exp(in\varphi)$, which are eigenstates of the orbital angular momentum operator [21]. The topological phase structure of these modes can be resolved experimentally using combinations of holographic and filtering techniques [1, 22], or interferometric methods [23]. The mode function given in equation (1) is naturally expressed in terms of eigenstates of the paraxial OAM operator, namely, the OAM content of the mode function that describes the signal photon. The OAM content [2] is given by the distribution C_n, where $C_n = \int_0^\infty \rho_k\,\mathrm{d}\rho_k\,|a_n(\rho_k)|^2$, and

$$a_n(\rho_k) = 1/(2\pi)^{1/2}\int_0^{2\pi}\mathrm{d}\varphi_k\,\Phi_s(\rho_k,\varphi_k)\exp(-\mathrm{i}n\varphi_k), \quad (8)$$

with $\rho_k = |\mathbf{p}|$ and $\varphi_k = \tan^{-1} p_y/p_x$ being the radius and azimuthal phase in cylindrical coordinates, respectively, of the transverse wavevector $\mathbf{p}$.

In figure 4 we plot the OAM content for some SPDC configurations with crystal length $L = 2$ mm and $l_0 = 1$. Figures 4(a)–(c) correspond to an angle of emission of $\varphi_1 = 1°$ and $\alpha = 0°$. For a beam width of $w_0 = 800\ \mu$m, which is plotted in figure 4(a) and whose spatial shape is plotted in figure 2(a), the OAM content shows a distribution highly peaked at $l_1 = 1$. The OAM content of the downconverted photons can change dramatically when modifying the beam

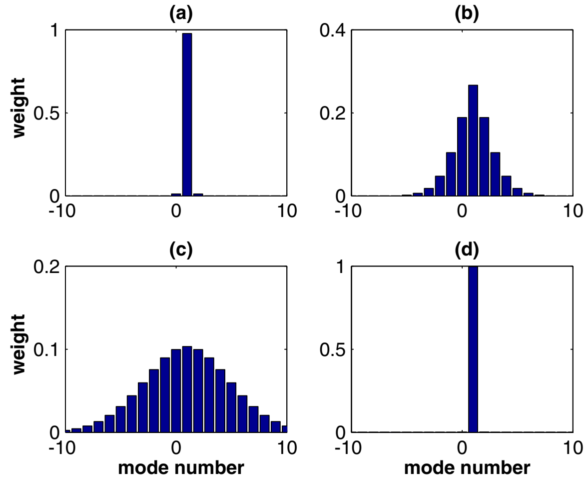

Figure 4. OAM content of the mode function of the signal photon. (a) $w_0 = 800\ \mu$m, $\alpha = 0°$, $\varphi_1 = 1°$, (b) $w_0 = 80\ \mu$m, $\alpha = 0°$, $\varphi_1 = 1°$, (c) $w_0 = 40\ \mu$m, $\alpha = 0°$, $\varphi_1 = 1°$, and (d) $w_0 = 40\ \mu$m, $\alpha = 90°$, $\varphi_1 = 5°$. Length of the crystal: $L = 2$ mm. Angle of emission of the downconverted photons: $\varphi_1 = -\varphi_2 = 1°$. Focal length of the 2-f system: $f = 25$ cm.

(This figure is in colour only in the electronic version)

width of the pump beam, as shown in figures 4(b) and (c). The OAM distribution plotted in figure 4(c) corresponds to the spatial shape plotted in figure 2(c). Only for large values of L_w and L_{nc}, when compared with the crystal length L, the OAM distribution of the signal photon shows mostly a single peak, according to the selection rule $l_0 = l_1 + l_2$, as is the case in some experiments [1, 12]. In some other experiments, the parameter space of the experimental configuration chosen determines a smaller value of L_{nc} or L_w, thus observing a non-centrosymmetric spatial shape of the signal photon [11, 13]. Therefore, the OAM distribution of the mode function of the signal photon contains many more modes, for which $l_0 \neq l_1 + l_2$. In figure 4(d) is shown the OAM content corresponding to the spatial shape plotted in figure 3(b), with $\alpha = 90°$ and $\varphi_1 = 5°$. Notice that although one has $L_w, L_{nc} < L$, the OAM distribution shows a single peak at $l_1 = 1$, due to the compensation of the non-collinear and spatial walk-off effects. The important practical implications of this result are readily apparent.

The main conclusion to be drawn from the previous results is that when implementing spatially encoded quantum information protocols based in OAM with strongly focused pump beams, or alternatively longer crystals, the specific properties afforded by walking entangled states cannot be avoided. As shown in figure 4, such properties are not necessarily detrimental. Notice also that strongly focused beams or longer crystals can be required to obtain a higher count rate of downconverted photons.

In summary, we have elucidated the spatial shape of entangled photon pairs generated by SPDC in different non-collinear geometries which also exhibit Poynting vector walk-off for some of the interacting waves. We found, in particular, that the OAM selection rule of entangled pairs generated in collinear SPDC, namely $l_0 = l_1 + l_2$, does not hold in general, even for nearly collinear geometries, when using strongly focused pump beams. Notwithstanding, under appropriate conditions that concern the geometric configuration of the SPDC process, the pump beam width, and the crystal length, it can be fulfilled. We notice that this is particularly important for the implementation of quantum information protocols based on spatially encoded information. The ellipticity of the spatial shape of the entangled photons is induced by the walk-off length of the pump beam, and by the non-collinear length. The importance of both effects is dictated by the length of the nonlinear crystal, and by the diffraction length of the pump beam, in sharp contrast to collinear phase matching with non-critical phase matching. We stress that the effects described here are directly relevant to current experiments [1, 11, 12].

Acknowledgments

This work was supported by the Generalitat de Catalunya and by grants BFM2002-2861 and FIS2004-03556 from the Government of Spain.

References

[1] Mair A, Vaziri A, Weihs G and Zeilinger A 2001 *Nature* **412** 313

[2] Molina-Terriza G, Torres J P and Torner L 2002 *Phys. Rev. Lett.* **88** 013601

[3] Vaziri A, Weihs G and Zeilinger A 2002 *Phys. Rev. Lett.* **89** 240401

[4] Molina-Terriza G, Vaziri A, Ursin R and Zeilinger A 2005 *Phys. Rev. Lett.* **94** 040501

[5] Molina-Terriza G, Vaziri A, Rehacek J, Hradil Z and Zeilinger A 2004 *Phys. Rev. Lett.* **92** 167903

[6] Langford N K, Dalton R B, Harvey M D, O'Brien J L, Pryde G J, Gilchrist A, Barlett S D and White A G 2004 *Phys. Rev. Lett.* **93** 053601

[7] Pittman T B, Strekalov D V, Klyshko D N, Rubin M H, Sergienko A V and Shih Y H 1996 *Phys. Rev.* A **53** 2804

[8] Migdall A 1997 *J. Opt. Soc. Am.* B **14** 1093

[9] Molina-Terriza G, Torres J P and Torner L 2003 *Opt. Commun.* **228** 155

[10] Torres J P, Osorio C I and Torner L 2004 *Opt. Lett.* **29** 1939

[11] Altman A R, Koprulu K G, Corndorf E, Kumar P and Barbosa G A 2005 *Phys. Rev. Lett.* **94** 123601

[12] Walborn S P, de Oliveira A N, Thebaldi R S and Monken C H 2004 *Phys. Rev.* A **69** 023811

[13] Joobeur A, Saleh B E A, Larchuk T S and Teich M C 1996 *Phys. Rev.* A **53** 4360

[14] Dmitriev V G, Gurzadyan G G and Nikogosyan D N 1997 *Handbook of Nonlinear Optical Crystals* (Berlin: Springer)

[15] Walborn S P, de Oliveira A N, Papua S and Monken C H 2003 *Phys. Rev.* A **90** 143601

[16] Torres J P, Alexandrescu A and Torner L 2004 *Phys. Rev.* A **68** 050301

[17] Franke-Arnold S, Barnett S M, Padgett M J and Allen L 2002 *Phys. Rev.* A **65** 033823

[18] Saleh B E A, Abouraddy A F, Sergienko A V and Teich M C 2000 *Phys. Rev.* A **62** 043816

[19] Kuklewicz C E, Fiorentino M, Messin G, Wong F N and Shapiro J H 2004 *Phys. Rev.* A **69** 013807

[20] Pelton M, Marsden P, Ljunggren D, Tengner M, Karlsson A, Fragemann A, Canalias C and Laurell F 2004 *Opt. Express* **12** 3573

[21] Allen L, Padgett M J and Babiker B 1999 *Progress in Optics* vol 39, ed E Wolf (Amsterdam: Elsevier) pp 291–372

[22] Bazhenov V Y, Vasnetsov M V and Soskin M S 1990 *JEPT Lett.* **52** 429

[23] Leach J, Padgett M J, Barnett S M, Franke-Arnold S and Courtial J 2002 *Phys. Rev. Lett.* **88** 257901